


REPLY

Impedance matching control between a human arm and a haptic joystick for long-term

Jiwook Choi, Zhanming Gu, Jangmyung Lee[†]  and Inho Lee*

Department of Electronics Engineering, Pusan National University, Busan 609-735, Korea

*Corresponding author. E-mail: inholee8@pusan.ac.kr

Received: 7 November 2020; **Revised:** 23 July 2021; **Accepted:** 30 August 2021; **First published online:** 25 October 2021

Keywords: human arm's impedance modeling, impedance estimation, impedance matching control, haptic joystick

Abstract

An impedance matching control framework between a human and a haptic joystick for long-term teleoperation is proposed in this research. An impedance model of the human arm is established analyzing the characteristics of human perception, decision, and action. The coefficients of the human arm's impedance have been identified using a least squares method. The human arm's impedance matching algorithm generates a corresponding motion vector for the human arm, which is determined by the interaction force measured by a force/torque sensor considering the impedance modeling of the human arm. The impedance control has been adopted for the haptic joystick to match the desired impedance to that of the human arm, which is aimed to minimize the energy consumption of the human arm for long-term teleoperation. By minimizing the fatigue of the operator, the remote control accuracy of the teleoperation can be improved. A PD control with gravity compensation algorithm has been adopted to maintain desired trajectory for the joystick by the operator more conveniently. The effectiveness of matching control has been demonstrated by trajectory following experiments for a mobile robot.

1. Introduction

The word “haptic” comes from the Greek word “haptesthai,” which means “to touch,” and indicates the ability to touch or manipulate objects. The haptic joystick is useful for an efficient remote control because it can generate operator commands and feedback the forces of the remote environment to the operator [1, 2]. In addition, it is necessary to design different types of haptic devices to meet the requirements of different control systems. Krishnan and Ganesh proposed a RRR three degree-of-freedom (DOF) parallel joystick that uses the motion constraint equation and the dynamic modeling of the motion platform to obtain the overall system dynamics equation of a parallel manipulator [3]. A haptic interface algorithm for a joystick to control a remote, unmanned vehicle was proposed [4]. The algorithm achieves effective remote control of unmanned vehicles. However, the accuracy of the output position of the joystick is insufficient since the feedback data are not accurate and fast enough for unmanned vehicles.

A 6-DOF haptic joystick structure was proposed to solve the problem of the accuracy of the joystick position output in 3D space [5]. However, the complicated structure causes the mechanical quality to be heavy, resulting in operator fatigue during long periods of operation and reducing work efficiency. To be an efficient human–computer interaction control, it is necessary to accurately identify the human body's motion intentions [6].

A bioelectrical signal can directly reflect human's motion intentions [7, 8]. For example, a surface electromyogram (SEMG) directly reflects the patient's muscle state, and an electroencephalogram (EEG) visually reflects the condition of the cerebral cortex-related area [9–12]. However, the analysis of bioelectrical signals requires a heavy computational burden and finally takes a long time to extract

[†] Deceased

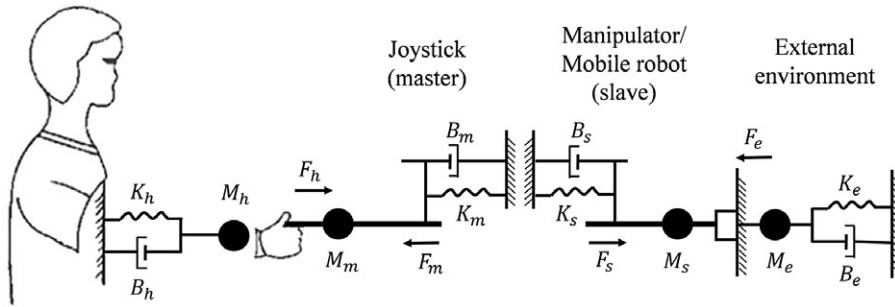


Figure 1. Schematic diagram of force feedback system.

the human’s motion intentions, which limits the approach to a slow and static working environment of a mobile robot.

To quantify human’s motion intention, this paper proposes a strategy that uses dynamic modeling of the human arm, as well as F/T (force/torque) sensor measurements, to calculate the motion vector for the joystick. Notice that it is difficult to obtain an accurate arm dynamic owing to the nonlinearity of the human arm itself. Various nonlinear controllers, compensation controllers, and neural network adaptive robust controllers can be used to compensate for nonlinear and uncertain factors of the dynamics.

Impedance control algorithms are widely used in human-in-loop human robot interaction systems (HIL-HRIS) [13–15]. The concept of this control algorithm was first proposed by Hogan [16], which is a generalization of damping control and rigid control. It was first implemented on the lower limb rehabilitation robot named “Lokomat” [17]. This algorithm can adaptively adjust the robot’s assisting force according to the residual muscle control ability of a patient’s central nervous system, so that the interaction between the robot and the patient is more coordinated and flexible. Ficuciello [18] proposed a variable impedance control algorithm based on a redundant manipulator, which improved the HRI performance and system stability through the fusion of a Cartesian impedance control regulator (CICR) and the redundant analysis method (RAM). This approach requires an expensive sensor and a complex redundant manipulator, which is limited to a very safe system with a compromise between better precision and execution efficiency [19].

Wang [20] proposed a new force position impedance controller for suppressing the position uncertainty during robot machining. This is applicable for cases in which the operator controls the manipulator through the joystick by impedance control, but the impedance of the human arm causes a loss in control accuracy. Artemiadis [21] proposed a 3D modeling method to estimate the impedance of a human arm. However, this method needs a strictly maintained experimental environment which requires expensive machinery. Li and Song [22] roughly estimated the human arm’s impedance using a least squares method, and the present study has optimized this method.

This paper proposes an impedance control strategy that matches the impedance of the operator’s arm to that of the joystick for more efficient and effortless long-term task execution. The composition of this paper is as follows: Section 2 introduces the basic structure of the impedance control system, Section 3 introduces the rationality of the human arm’s impedance modeling proposed in this paper from a physiological perspective. Section 4 presents the algorithm for estimation of the human arm’s impedance and impedance control strategy of the joystick to help the operator work efficiently and effortlessly. Section 5 presents the experimental results, and Section 6 concludes the paper.

2. Force feedback system based on impedance control

The overall schematic diagram of the force feedback system based on impedance control is shown in Fig. 1. F_h is the human arm’s force, F_m is the force exerted by the master on the human arm, F_s and F_e are the interaction forces between slave and external environment, K_h , B_h , and M_h are the human arm’s mass, damping, and stiffness coefficients, respectively. K_m , B_m , and M_m are the master’s mass, damping,

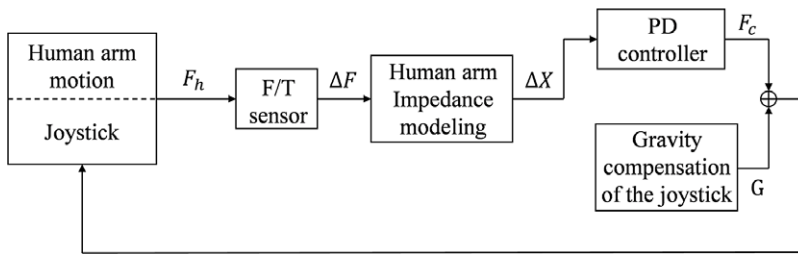


Figure 2. Block diagram of the impedance matching control system.

and stiffness coefficients, respectively. K_s and B_s are the slave's damping and stiffness. K_e , B_e , and M_e are the external environment's mass, damping, and stiffness coefficients, respectively.

The operator manipulates the joystick (master) to control the manipulator or to generate the commands for a mobile robot (slave), and the interaction force generated when the manipulator touches the external environment is fed back to the operator through the joystick. This paper focuses on the efficiency of the operator's manipulation of the joystick and thus only discusses the control strategy of the joystick. The goal is efficient and effortless joystick manipulation by the operator during long-term operation. To achieve this goal, it is necessary for the joystick to generate a compensation force to help the operator. By the impedance matching control between the impedance of the human arm and the joystick, the human operator becomes very comfortable operating the joystick.

In Fig. 2, ΔF is the interaction force between the human arm and the joystick. The F/T sensor has been used to measure the human operator's force, F_h , which can be used to represent the human intention. ΔX is the position increment calculated from the human arm's impedance modeling defined as $\Delta F / \Delta X$. F_c and G are the force generated by PD controller and the gravity compensation force, respectively. With this gravity compensation, the fatigue of human operators for long-term teleoperation can be reduced.

3. Dynamic modeling of human arm

The operator receives a variety of sensory stimuli during manipulation of the joystick, and the feedback information can be classified into two information types: force feedback and position feedback. This is a complex process by which the operator perceives the environment to make decisions based on the force and position feedback information provided by the multisensory stimulus. However, according to the results of the operator's decision, this decision process can be classified into two modes: force command mode and position command mode. The force command mode can be used when the operator wants to keep a constant force. The position command mode includes majority of human commands to move to the desired position.

To establish dynamic modeling of the human arm, it is necessary to deeply understand the characteristics of the human arm from the brain's decision to the arm muscle's motion. For the convenience of research, this study established the operator's layered dynamics modeling from a physiological point of view. This modeling consists of the decision, fusion, and conduction layers, as well as the arm [23].

Figure 3 shows the whole process from a human's decision to act, and the action has been divided into 2 modes: force command mode and position command mode. k_p and k_f are the zero-frequency gains of position and force, respectively. T_p and T_{pl} represent the prediction and lag factors, respectively, in the operator's position command process. T_f and T_{fl} represent the operator's prediction and lag factors, respectively, in the force command process. $r_p(n)$, $r_f(n)$, and $r(n)$ are the white noises and Z_h represents the impedance modeling of the human arm.

3.1. Decision layer

There are two command modes generated by the decision layer for the control of the mobile robot: force and position commands modes. Force command mode: This mode corresponds to a completely

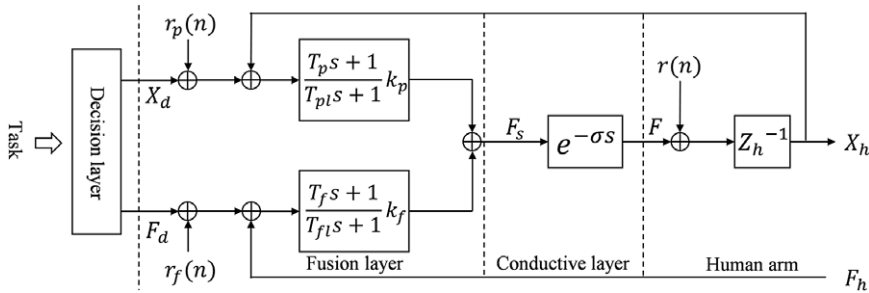


Figure 3. Diagram of operator's layered dynamics modeling.

restricted mode, that is, the human brain converts the task into a certain desired force output according to the situation of the object in the environment. The desired position is set to be equal to the actual position of the human hand, that is,

$$X_d = X_h \tag{1}$$

where X_d and X_h are the desired and current human hand's positions, respectively.

Position command mode: This mode corresponds to the free motion mode, that is, the human brain converts the task into a certain desired position output according to the situation of the object in the environment, and the expected force is equal to the actual force of the human hand, that is,

$$F_d = F_h \tag{2}$$

where F_d and F_h are the desired and actual human hand's forces, respectively.

3.2. Fusion layer

In the fusion layer, the operator's positioning process and force determination process are fused. The output force at the fusion layer, F_s , can be obtained in s domain as follows:

$$F_s(s) = \frac{T_p s + 1}{T_{pl} s + 1} k_p e_p(s) + \frac{T_f s + 1}{T_{fl} s + 1} k_f e_f(s) \tag{3}$$

where $e_p(s) = X_d(s) - X_h(s) + r_p(n)$, $e_f(s) = F_d(s) - F_h(s) + r_f(n)$, $r_p(n)$ and $r_f(n)$ are the white noises generated from the contacted object's position and force errors, respectively, which are very small to be eliminated without any problem [24].

3.3. Conductive layer

In the conductive layer, a value obtained by applying the delay time of nerve transmission is transmitted to the movement of the human arm. The output force at the conductive layer, F_c , can be described as

$$F(s) = F_s(s) e^{-\sigma s} \tag{4}$$

where σ [second] represents the time delay of the transmission nerves.

3.4. Human arm's motion

The human arm's motion after the gravity compensation in Fig. 2 can be described using the impedance modeling as follows:

$$\begin{aligned}
 F(s) + r(n) &= (M_h s^2 + B_h s + K_h) \cdot X_h(s) \\
 &= Z_h \cdot X_h(s),
 \end{aligned}
 \tag{5}$$

where $r(n)$ is the white noise caused by muscle fatigue, which can be negligible; M_h , B_h , and K_h care the mass, damping, and stiffness coefficients of the human arm, respectively.

From Fig. 3, $F(s)$ can be obtained after the blocks of $G_p(s)$ and $G_f(s)$. As a result Equation (5) can be represented as follows:

$$G_p(s)(X_d(s) - X_h(s)) + G_f(s)(F_d(s) - F_h(s)) = Z_h \cdot X_h(s)
 \tag{6}$$

where $G_p(s)$ and $G_f(s)$ are obtained from Fig. 3 as follows:

$$G_p(s) = \frac{T_p s + 1}{T_{pl} s + 1} k_p e^{-\sigma s}
 \tag{7}$$

$$G_f(s) = \frac{T_f s + 1}{T_{fl} s + 1} k_f e^{-\sigma s}
 \tag{8}$$

$G_p(s)$ is a position factor and $G_f(s)$ is a force factor. When the operator works in position command mode, the position prediction factor becomes the dominant factor in determining human motion and other factors can be eliminated. That is, $G_p(s)$ and $G_f(s)$ can be simplified ignoring the delay time and the lag factors, T_{pl} and T_{fl} , which can be approximated to be zero. Also the force prediction factor, T_f , can be eliminated. Equations (7) and (8) can be simplified as follows:

$$G_p(s) = (T_p s + 1) k_p
 \tag{9}$$

$$G_f(s) = k_f
 \tag{10}$$

As the result, the Eq. (6) can be presented as follows:

$$(T_p s + 1) k_p (X_d(s) - X_h(s)) + (F_d(s) - F_h(s)) = Z_h X_h
 \tag{11}$$

According to the neurophysiology research results [25], the response time distribution of the operator in the processes of perception, decision, and control is as follows: the process by which the receptor transforms the stimulus into a nerve impulse needs 1 to 38 ms, and the nerve-conduction process needs 2 to 100 ms. The neural decision-making process requires 70 to 300 ms, and the process by which the efferent nerve transmits the command to the neuro muscle requires 10 to 20 ms.

As the operating frequency of the human robot interaction system is affected by the operating bandwidth of the actuator, it generally works in the low frequency region. Some factors can be ignored to simplify the operator arm's dynamic modeling and the modeling can be represented as follows:

$$\begin{aligned}
 F_h(s) &= (M_h s^2 + B_h s + K_h) \cdot \Delta X(s) \\
 &= Z_h \cdot \Delta X(s).
 \end{aligned}
 \tag{12}$$

This modeling can also be called an impedance modeling. The joystick occupies a 3D space, and thus F_h and $\Delta X \in \square^{3 \times 1}$, Z_h, M_h, B_h , and $K_h \in \square^{3 \times 3}$.

4. Joystick impedance control

4.1. Human arm impedance estimation

To determine the impedance coefficients of the human arm, the operator works in the position command mode. At this time, X_d is a preset reference path and only the operator arm's impedance coefficients in this

reference path can be estimated because the arm’s impedance changes with muscle contractions [26]. F/T sensor is used to measure the interaction force between the human hand and the joystick. Based on the interaction force between the hand and joystick measured by the F/T sensor and the position increment calculated by the angles measured by the encoders, the impedance coefficients of the human arm can be obtained as follows:

$$Z_h = \frac{F_h}{\Delta X} \tag{13}$$

If $F_h(x, y, z)$ can be expressed as a differentiable nonlinear function of the position of the end point of the human arm as follows:

$$dF_i = \left(\frac{\partial F_i}{\partial x} \right) dx + \left(\frac{\partial F_i}{\partial y} \right) dy + \left(\frac{\partial F_i}{\partial z} \right) dz \tag{14}$$

where $i = x, y,$ and z which are the coordinates of the end point of the human arm in a 3D space. Notice that the human arm’s impedance can be expressed as a differential operator and is associated with infinitesimal force changes and infinitesimal displacements.

Equation (14) is correct only in the case of infinitesimal displacements. Therefore, a reliable method is measuring the force of many discontinuous points and then estimating the coefficients of the human arm’s impedance modeling by processing the obtained data.

The impedance modeling proposed in the previous section is represented as follows:

$$F_h = M_h (\ddot{X}_c - \ddot{X}_d) + B_h (\dot{X}_c - \dot{X}_d) + K_h (X_c - X_d) \tag{15}$$

where X_d and X_c represent the desired and actual positions, respectively; \dot{X}_c and \ddot{X}_c are the actual velocity and acceleration of the arm, respectively; \dot{X}_d and \ddot{X}_d are the desired velocity and acceleration of the arm, respectively.

Assuming that the operator’s hand applies a force dF_h to the joystick over a very short time, which causes the joystick to move a very short distance dX_h , the impedance modeling can be defined as follows:

$$F_h + dF_h = M_h(\ddot{X}_c + d\ddot{X}_h - \ddot{X}_d) + B_h(\dot{X}_c + d\dot{X}_h - \dot{X}_d) + K_h(X_c + dX_h - X_d), \tag{16}$$

where $dX_h, d\dot{X}_h,$ and $d\ddot{X}_h$ are the distance, velocity, and acceleration of the arm’s motion over a short time, respectively. By subtracting Eq. (15) from Eq. (16), dF_h can be expressed as follows:

$$dF_h = M_h d\ddot{X}_h + B_h d\dot{X}_h + K_h dX_h. \tag{17}$$

Assuming that \hat{F}_h is the estimated force output of the human hand, $\hat{M}_h, \hat{B}_h,$ and \hat{K}_h are the estimated values of the arm’s mass, damping, and stiffness coefficients, respectively. The human arm’s force, $\hat{F}_h,$ can be represented as follows:

$$\hat{F}_h = \hat{M}_h \ddot{X} + \hat{B}_h \dot{X} + \hat{K}_h X. \tag{18}$$

By using the least squares method, square error S can be expressed as follows:

$$S = \sum_{p=1}^n \left[F_h(p) - \hat{F}_h(p) \right]^2 \tag{19}$$

Notice that $\frac{\partial S}{\partial \hat{M}_h}, \frac{\partial S}{\partial \hat{B}_h},$ and $\frac{\partial S}{\partial \hat{K}_h}$ can be approximated as zeros [22]. Using the Eq. (18) and (19), impedance coefficients of human arm can be estimated as follows:

$$\begin{bmatrix} \hat{M}_h \\ \hat{B}_h \\ \hat{K}_h \end{bmatrix} = \begin{bmatrix} \sum_{p=1}^n \ddot{X}^2(p) & \sum_{p=1}^n \ddot{X}(p)\dot{X}(p) & \sum_{p=1}^n \ddot{X}(p)X(p) \\ \sum_{p=1}^n \dot{X}(p)\ddot{X}(p) & \sum_{p=1}^n \dot{X}^2(p) & \sum_{p=1}^n \dot{X}(p)X(p) \\ \sum_{p=1}^n X(p)\ddot{X}(p) & \sum_{p=1}^n X(p)\dot{X}(p) & \sum_{p=1}^n X^2(p) \end{bmatrix}^{-1} \cdot \begin{bmatrix} \sum_{p=1}^n \ddot{X}(p)F_h(p) \\ \sum_{p=1}^n \dot{X}(p)F_h(p) \\ \sum_{p=1}^n X(p)F_h(p) \end{bmatrix} \tag{20}$$

where n is the number of sampling points and t is the sampling time.

To estimate the time-varying impedance coefficients of the human arm in a short time, the impedance can be represented as follows:

$$\hat{Z}_h(t) = V(t)^{-1}W(t) \tag{21}$$

where
$$V(t) = \begin{bmatrix} \sum_{p=t-n+1}^n \ddot{X}^2(p) & \sum_{p=t-n+1}^n \ddot{X}(p)\dot{X}(p) & \sum_{p=t-n+1}^n \ddot{X}(p)X(p) \\ \sum_{p=t-n+1}^n \dot{X}(p)\ddot{X}(p) & \sum_{p=t-n+1}^n \dot{X}^2(p) & \sum_{p=t-n+1}^n \dot{X}(p)X(p) \\ \sum_{p=t-n+1}^n X(p)\ddot{X}(p) & \sum_{p=t-n+1}^n X(p)\dot{X}(p) & \sum_{p=t-n+1}^n X^2(p) \end{bmatrix}$$
 and
$$W(t) = \begin{bmatrix} \sum_{p=t-n+1}^n \ddot{X}(p)F_h(p) \\ \sum_{p=t-n+1}^n \dot{X}(p)F_h(p) \\ \sum_{p=t-n+1}^n X(p)F_h(p) \end{bmatrix}.$$

Notice that n is the number of samples and is set to 150 experimentally considering the control cycle. The elements of $V(t)$ and $W(t)$ can be estimated by the simulated annealing (SA) method as follows [27]:

$$\begin{aligned} v_{p,q}(t+1) &= \sum_{i=t-n+2}^n X^{(3-p)}(i)X^{(3-q)}(i) \\ &= v_{p,q}(t) + X^{(3-p)}(t+1)X^{(3-q)}(t+1) - X^{(3-p)}(t-n+1)X^{(3-q)}(t-n+1), \end{aligned} \tag{22}$$

where $p = 1, 2, 3$ and $q = 1, 2, 3$.

$$w_p(t+1) = \sum_{i=t-n+2}^n X^{(3-p)}(i)F_h(i) = w_p(t) + X^{(3-p)}(t+1)F_h(t+1) - X^{(3-p)}(t-n+1)F_h(t-n+1). \tag{23}$$

where $p = 1, 2, 3$.

The resulting matrix can be approximated to a diagonal matrix to observe the changes in the human arm’s impedance.

4.2. Impedance control of joystick

The estimated human arm’s impedance has been matched to that of the joystick during the control of the joystick. This joystick used in this research is a parallel structure consisting of three serial manipulators, as shown in Fig. 4.

Each serial manipulator consists of two active joints and one passive joint; the gray joints are the active joints and the white joint is the passive joint. Three serial manipulators with 3-DOF are connected to the upper plate by passive spherical joints, and the motions of the serial manipulators generate the motion of the upper plate relative to the lower plate.

Figure 5 shows related angles in kinematic analysis of one of the serial manipulators. Because the joystick consists of three serial manipulators in parallel, the position of each joint point on the upper plate is identical to the position of the end effector of each serial manipulator. Therefore, if the positions of the end effectors of the three series manipulators are obtained, the coordinates of the central position can be obtained by finding the average of the coordinates of the three points. Thereafter, the position and direction of movement of the upper plate can be derived.

Table I shows the link parameter table for the serial manipulator in Fig. 5. The a value of the DH parameter is length of the common normal, d is offset along previous z to the common normal, α is

Table I. Denavit–Hartenberg parameter of each serial manipulator.

Link	a	d	α	θ
1	0	0	$\pi/2$	θ_{1i}
2	l_1	0	0	θ_{2i}
3	l_2	0c	0	θ_{3i}

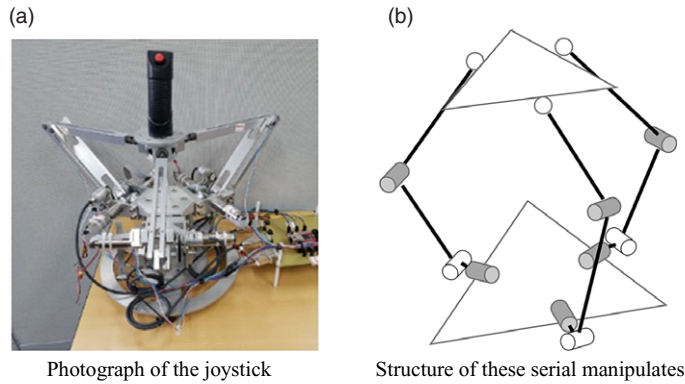


Figure 4. Joystick in this research.

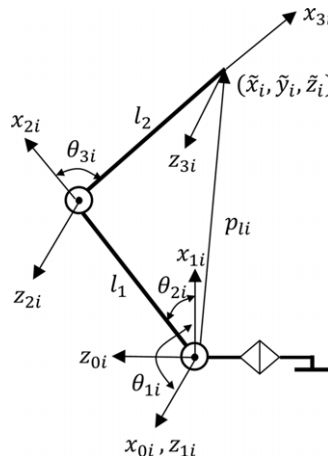


Figure 5. Link parameters of a serial manipulator.

angle about common normal, from $z_{i-1}c$ to z_i and θ is angle about previous z , from x_{i-1} to x_i . The position kinematic equations for the manipulator can be obtained as follows:

$$\begin{bmatrix} \hat{X}_i \\ \hat{Y}_i \\ \hat{Z}_i \end{bmatrix} = \begin{bmatrix} l_1 \cos(\theta_{2i}) + l_2 \cos(\theta_{2i} + \theta_{3i}) \\ \sin(\theta_{1i})(l_1 \sin(\theta_{2i}) + l_2 \sin(\theta_{2i} + \theta_{3i})) \\ l_1 \cos(\theta_{1i}) \sin(\theta_{2i}) + l_2 \cos(\theta_{1i}) \sin(\theta_{2i} + \theta_{3i}) \end{bmatrix} \tag{24}$$

The position of the haptic joystick’s end effector is considered to be the center of the upper plate and is marked as X. The prediction of the target position is based on the force in the x-y-z directions sensed by the F/T sensor and the previously estimated human arm’s impedance coefficients. The differential equation is solved and the required position increments in the x-y-z directions are obtained. This joystick can be controlled by dynamic modeling as follows:

$$M_h (\ddot{X}_c - \ddot{X}_d) + B_h (\dot{X}_c - \dot{X}_d) + K_h (X_c - X_d) = F. \tag{25}$$

With the definition of $\Delta X = X_c - X_d$, which represents the position increment caused by human’s motion intention, Eq. (25) can be represented as

$$\Delta \ddot{X} + M_h^{-1} B_h \Delta \dot{X} + M_h^{-1} K_h \Delta X = M_h^{-1} F. \tag{26}$$

The analytical solution of differential Eq. (26) can be obtained ignoring the initial conditions as follows:

$$\Delta X = e^{-\lambda_1 t} + e^{-\lambda_2 t} + K_h^{-1} F \tag{27}$$

where λ_1 and λ_2 are the general solutions of the following characteristic equation:

$$\lambda^2 + M_h^{-1} B_h \lambda + M_h^{-1} K_h = 0 \tag{28}$$

To manipulate this joystick to follow the human hand compliantly, a PD control with the gravity compensation algorithm has been adopted to drive all the motor parameters in the joystick. The designed controller can be represented as

$$F_c = K_p \Delta X + K_D \Delta \dot{X} + G(\theta) \tag{29}$$

where K_p and K_D are the controller gains, ΔX is the position increment, and $G(\theta)$ is the gravity compensation force.

To obtain the gravity term, it is crucial to determine the mapping relationship between the gravity force and joint configuration. Considering that all joints of the joystick are revolute joints, if link p ’s center of mass is located at a point in link p , gravity $G(\theta)$ can be expressed as

$$G(\theta) = g(\theta)A \tag{30}$$

where $g(\theta)$ is the gravity acceleration on each link, which can be expressed as follows:

$$g(\theta) = \begin{bmatrix} g_{11}(\theta) & g_{12}(\theta) & \dots & g_{1(n-1)}(\theta) & g_{1n}(\theta) \\ 0 & g_{22}(\theta) & \dots & g_{2(n-1)}(\theta) & g_{2n}(\theta) \\ \dots & \dots & \dots & \dots & \dots \\ 0 & 0 & \dots & g_{(n-1)(n-1)}(\theta) & g_{(n-1)n}(\theta) \\ 0 & 0 & \dots & 0 & g_{nn}(\theta) \end{bmatrix} \tag{31}$$

Each element in matrix $g(\theta)$ can be calculated by

$$g_{pq}(\theta) = g(\partial R_0^p / \partial \theta_p) u_p \tag{32}$$

where $g = [0, 0, 9.8]^T m/s^2$, R_0^p is the rotation matrix of coordinate system p with respect to coordinate system 0, u_p is the coordinate system p ’s directional unit vector that points to link p ’s mass center.

In Eq. (30), A , a constant matrix, which is represented as follows:

$$A = \begin{bmatrix} m_1 l_1^c + l_1 \sum_{i=2}^n m_i \\ m_2 l_2^c + l_2 \sum_{i=3}^n m_i \\ m_3 l_3^c + l_3 \sum_{i=4}^n m_i \\ \dots \\ m_{n-1} l_{n-1}^c + l_{n-1} m_n \\ m_n l_n^c \end{bmatrix} \tag{33}$$

where l_p^c is the distance between coordinate system p ’s origin and link p ’s mass center, m_i is the mass of link i , and l_p is the distance between coordinate system p ’s origin and coordinate system $p + 1$ ’s origin.

Table II. Interaction force in the x, y and z directions before and after using the impedance matching algorithm.

	X Direction		Y Direction		Z Direction	
	After	Before	After	Before	After	Before
Average force (N)	1.178	0.189	1.102	0.168	0.592	0.079
Maximum force (+) (N)	2.873	0.791	3.831	0.746	1.259	0.203
Maximum force (−) (N)	3.225	0.661	2.561	0.553	1.135	0.274

5. Impedance matching and tracking experiments

5.1. Human arm's impedance estimation experiment

The following experiment is conducted to obtain the coefficients of the human arm's impedance modeling. A subject is a 25-year-old man with no disabilities. The subject sits on the chair and holds the handle and moves the joystick along the target trajectory with only gravity compensation. The target trajectory is a square with a side length of 0.3 m, centered on the initial position of the handle. The four vertices of the square are A, B, C, and D, respectively. The data collected are used to estimate the impedance of the human arm.

The data are sampled and stored for offline analysis. The data include the joystick joint angles and the forces in the x–y–z directions. The position of the joystick's end effector is calculated by considering the joint angles in the kinematic equation of the joystick. Details regarding the kinematics of the joystick are described in Section 5. The impedance coefficients obtained by the least squares method are shown in Fig. 6.

These figures show that the impedance of the human arm changes with the movement of the arm. Therefore, it is necessary to perform a real time impedance control to accurately match the desired impedance to the human arm's impedance during the joystick control.

5.2. Human motion prediction and reaction experiment

The estimated human arm's impedance coefficient is applied to the joystick impedance control to confirm the efficiency. The operator holds the handle and moves the joystick along the target trajectory. During this process, the force applied by the operator to the joystick is included in the impedance modeling to determine the target position, which is the target position at which the human brain sends a motion command to the arm through the nerve. The target position is a motion vector indicating the position increments in the x, y, and z directions. The designed PD controller with gravity compensation drives the motor settings in the joystick to allow the end effector to follow the guidance or traction of the operator's hand. The F/T sensor disposed at the end effector of the joystick senses the interaction force between the operator's hand and the joystick. The position of the joystick's end effector is transmitted to the mobile robot through the communication module to control the movement of the mobile robot. The position of the joystick's end effector has been calculated using the encoder recording angle and the link length, which has been used to calculate the trajectory tracking error against the reference trajectory.

Figure 7 shows the interaction forces between the operator's hand and the joystick before and after applying the impedance matching algorithm. It can be observed that the average values of the interaction force in the x, y, z directions become very small after applying the impedance matching algorithm. The specific values are shown as follows:

Table II shows the average interaction forces in x, y, z directions after applying the impedance matching algorithm, respectively. Notice that the interaction force becomes almost 7 times smaller by applying the impedance matching algorithm. The maximum forces in x, y, z directions after applying the impedance matching algorithm become 4 to 5 times smaller than before.

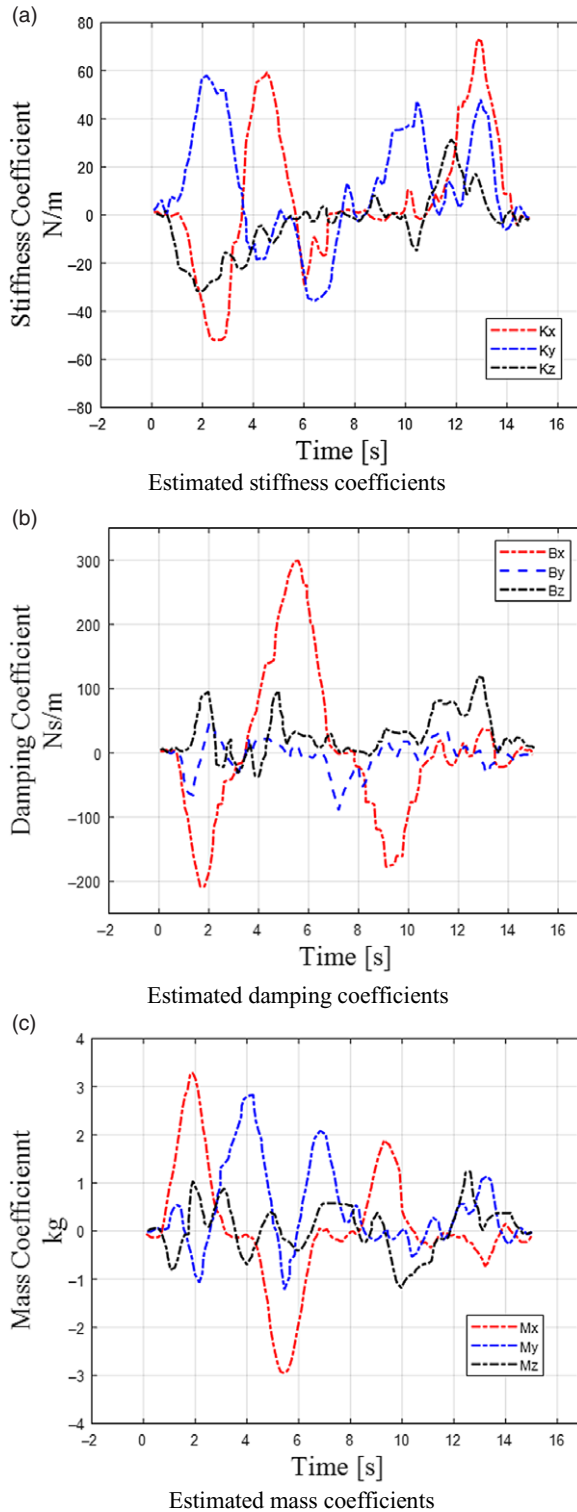
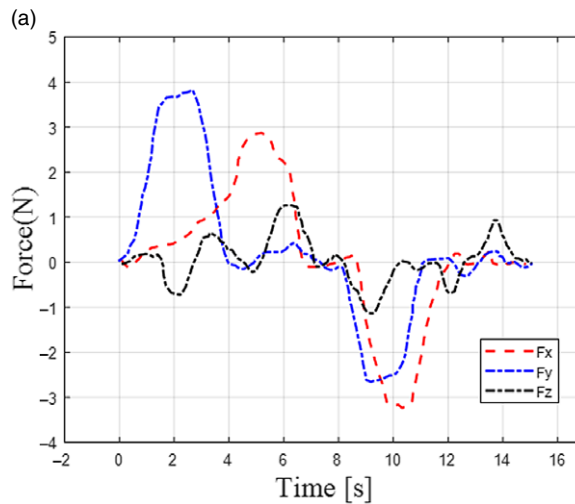


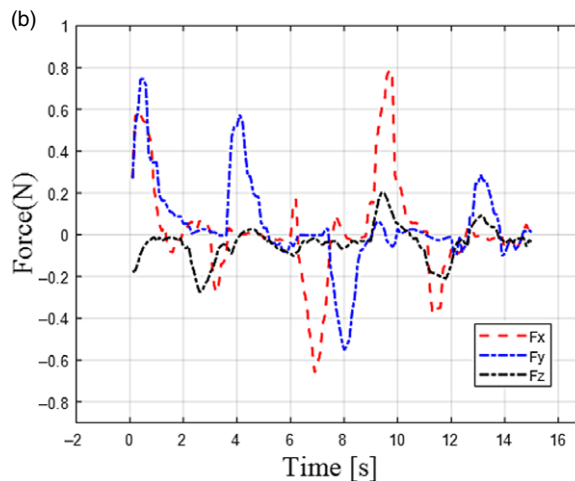
Figure 6. Estimated human arm's impedance coefficients.

Table III. Trajectory tracking accuracy.

	X Direction	Y Direction	Z Direction
Actual trajectory error (m)	0.021	0.019	0.015



Interaction forces without impedance matching



Interaction forces with impedance matching

Figure 7. Interaction forces before and after applying impedance matching algorithm.

Figure 8 shows the desired trajectory calculated from the estimated human arm’s impedance modeling and the actual trajectory in the impedance matching algorithm. It can be quantified that the average values of the trajectory tracking error are shown in Table III. In the experiment, there are three paths: square reference path (represented by A, B, C and D points), desired trajectory calculated by impedance model and force and real trajectory actuated by motors in the joystick. Through Figure 8 and Table III, the error values between the desired trajectory and the reference path occurred as much as 0.015 m, 0.012 m, and 0.011 m.

By the impedance matching control, the interaction force between the human and the joystick becomes 5 times smaller with the tracking error of 0.02m compared to the PD control without impedance matching. This proves the effectiveness of the human arm’s impedance matching algorithm proposed in this research.

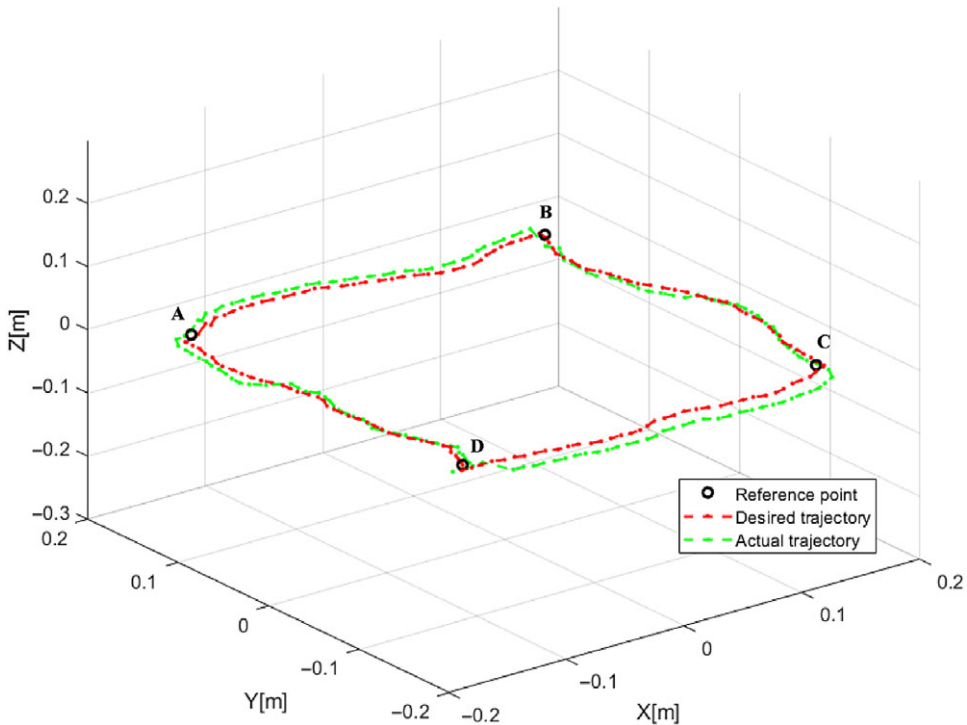


Figure 8. Trajectory tracking performance.

6. Conclusion

An impedance matching control strategy has been proposed and implemented to help operators in manipulating joysticks efficiently and effortlessly for long-term teleoperation. An impedance modeling of the human arm was obtained by estimating its impedance coefficients. The human arm's impedance modeling has been utilized under the control of the joystick to generate a force that conforms to the human's motion intention which completes the task. By this process, the impedances of the joystick and human arm are matched to each other. The effectiveness of the proposed algorithm has been demonstrated by the teleoperated trajectory following the operation of a mobile robot. By the impedance matching control, the interaction force between the human and the joystick becomes 5 times smaller with the tracking error of 0.02 m compared to the PD control without impedance matching. As future research, a machine learning algorithm can be adopted for identifying the human arm impedance coefficients, which improves the efficiency of the proposed control further.

Acknowledgments. This work has supported by the National Research Foundation of Korea (NRF) grant funded by the Korea government (No. 2021R1C1C1009989). This work was supported by BK21PLUS, Creative Human Resource Education and Research Programs for ICT Convergence in the 4th industrial Revolution. This research was supported by the National Research Foundation of Korea (NRF) grant funded by the Korea government (MSIT) (No. 2020R1A6A3A13072460).

References

- [1] A. Takemoto and K. Yano, "Obstacle avoidance control system of rotary crane using proposed haptic joystick," in *World Haptics Conference* (IEEE press, Pisa, Italy, 2005), pp. 22–23.
- [2] Q. Qin and I. Yutaka, "Softness Comparison of Stabilization Control in Remote Robot System with Force Feedback," *TENCON 2018 IEEE Region 10 Conference* (IEEE press, Jeju, Korea, 2018), pp. 32–37.

- [3] K. R. R. Krishnan and M. Ganesh, “Reshaping the Singularities in 3 D.O.F 3-RRR Planar Parallel Manipulator by Varying the Position of the Actuator,” *Int. Conf. on Robotics: Current Trends and future Challenges (RCTFC)* (IEEE Press, India, Thanjavur, 2016), pp. 37–42.
- [4] S. K. Cho and H. Z. Jin, Teleoperation of a mobile robot using a force-reflection joystick with sensing mechanism of rotating magnetic field, *IEEE/ASME Trans. Mechatronics*, **15**(1), 17–26 (2010).
- [5] S. S. Lee and J. M. Lee, “Design of a general purpose 6-DOF haptic interface,” *Mechatronics*, **13**(7), 697–722 (2003).
- [6] J. Huang and W.-G. Huo, “Control of upper-limb power-assist exoskeleton using a human-robot interface based on motion intention recognition,” *IEEE Trans. Autom. Sci. Eng.* **12**(4), 1257–1270 (2003).
- [7] L.-N. Tong and Z.-G. Hou, “Multi-channel sEMG time series analysis based human motion recognition method,” *Acta Automatica Sinica* **40**(5), 810–821 (2014).
- [8] J. G. Ngeo and T. Tamei, “Continuous and simultaneous estimation of finger kinematics using inputs from an EMG-to-muscle activation model,” *J NeuroEng. Rehabil.* **11**(122), 1–14 (2014).
- [9] J. Hashemi and E. Morin, “Enhanced dynamic EMG-force estimation through calibration and PCI modeling,” *IEEE Trans. Neural Syst. Rehabil. Eng.* **23**(1), 41–50 (2015).
- [10] N. Parajuli and P. Bifulco, “Real-time EMG based pattern recognition control for hand prostheses: A review on existing methods, challenges and future implementation,” *Sensors* **19**(20), 15–23 (2019).
- [11] M. Mulas and M. Folgheraiter, “An EMG-Controlled Exoskeleton for Hand Rehabilitation,” *Int. Conf. on Rehabilitation Robotics (ICORR)* (IEEE press, Chicago, USA, 2005), pp. 371–374.
- [12] E. Scheme and K. Englehart, “Electromyogram pattern recognition for control of powered upper-limb prostheses: state of the art and challenges for clinical use,” *J. Rehabil. Res. Dev.* **48**(6), 643–659 (2011).
- [13] J. C. P. Ibarra and A. A.-G. Siqueira, “Impedance Control of Rehabilitation Robots for Lower Limbs, Review,” *Conf. on Robotics: SBR-LARS Robotics Symposium and Robo-control* (IEEE Press, Sao Carlos, Brazil, 2014), pp. 235–240.
- [14] Y. N. Li and W. He, “Neural network control of a rehabilitation robot by state and output feedback,” *J. Intell. & Rob. Sys.* **80**(1), 15–31 (2015).
- [15] S. A. Napper and R. L. Seaman, “Applications of robots in rehabilitation,” *Robot. Auton. Syst.* **5**(3), 227–239 (1989).
- [16] N. Hogan, “Impedance Control: An Approach to Manipulation,” *1984 American Control Conference* (IEEE Press, San Diego, USA, 1984), pp. 304–313.
- [17] M. Bernhardt and M. Frey, “Hybrid Force-Position Control Yields Cooperative Behavior of the Rehabilitation Robot LOKOMAT,” *Int. Conf. on Rehabilitation Robotics (ICORR)* (IEEE Press, Chicago, USA, 2005), pp. 536–539.
- [18] F. Ficuciello and A. Romano, “Cartesian Impedance Control of Redundant Manipulators for Human-Robot Co-Manipulation,” *Int. Conf. on Intelligent Robots and Systems* (IEEE Press, Chicago, USA, 2014), pp. 2120–2125.
- [19] F. Ficuciello and A. Romano, “Variable impedance control of redundant manipulators for intuitive Human–Robot physical interaction,” *IEEE Trans. Robot.* **31**(4) (2015) pp. 850–863.
- [20] X. L. Wang, “Force Estimation Based Position Impedance Control for Robotic Machining Process,” *Int. Conf. on Mechanic Automation and Control Engineering* (IEEE Press, Wuhan, China, 2010), pp. 37–40.
- [21] P. K. Artemiadis and P. T. Katsiaris, “Human Arm Impedance: Characterization and Modeling in 3D Space,” *Int. Conf. on Intelligent Robots and Systems* (IEEE Press, Taipei, Taiwan, 2010), pp. 3103–3108.
- [22] H. J. Li and A. G. Song, “Virtual-environment modeling and correction for force-reflecting teleoperation with time delay,” *IEEE Trans. Ind. Electron.* **54**(2), 1227–1233 (2007).
- [23] H. S. Kook and S. Kota, “A Dynamic Multi-Channel Decision-Fusion Strategy to Classify Differential Brain Activity,” *Int. Conf. of the IEEE Engineering in Medicine and Biology Society* (IEEE Press, Louisville, USA, 2007), pp. 3212–3215.
- [24] C. Talukdar and R. Barman, “Analysis of noise and its removal in nerve conduction study signal,” *Int. Conf. on Innovations in Electronics, Signal Processing and Communication (IESC)* (IEEE Press, Louisville, Shillong, India, 2017), pp. 143–148.
- [25] D. M. Merfeld and T. K. Clark, “Dynamics of individual perceptual decisions,” *IEEE Trans. Robot.* **115**(1), 39–59 (2016).
- [26] F. Atsushi and O. Shohei, “A Muscle Tension Estimation Method by using Mechanical Impedance of Human Knee Joint During Training by Manipulator,” *Int. Conf. on Mechatronics* (IEEE Press, Changchun, China, 2007), pp. 1–6.
- [27] A. Song, L. Pan, G. Xu and H. Li, “Impedance identification and adaptive control of rehabilitation robot for upper-limb passive training, foundations and applications of intelligent systems,” *Adv. Intell. Syst. Comput.* **213**, 691–710 (2013).